Supplementary Material

S1 Effect of the fluid model assumption on a single-node asymmetric bifurcation

Expanding on section 2.3 of the main text, we conducted a sensitivity analysis on a simple asymmetric parent-daughter bifurcation with a single vascular node (Figure S1). For that, we used the Hagen-Poiseuille model with hematocrit, without and with backflow (sections S1.1, S1.2, respectively), a power law fluid model (section S1.3) and the Carreau model (section S1.4) which accounts for the non-Newtonian shear thinning behaviour of blood. In each case, we apply the conservation of flux, which is simply an extension of mass conservation, as well as the continuity of pressure at the bifurcation node, denoted in Figure S1 by $P*$ to solve a system of equations. The individual impedances and compliances calculated for each blood vessel are provided in Table S2 [1, 2].

S1.1 Hagen-Poiseuille model without backflow

Node-to-node pressure gradient calculation: For a steady laminar axisymmetric fully developed flow, the Navier-Stokes equations in cylindrical coordinates (r, θ, x) can be reduced, with the assumption that $u_r = u_\theta = 0$, to an axial momentum equation with velocity $u(x) = u_x$ as a function only of the spatial coordinate x for the length of the cylindrical blood vessel, which can be written as

$$\frac{1}{r}\frac{\partial}{\partial r}\left(r\frac{\partial u}{\partial r}\right) = \frac{1}{\mu}\left(\frac{dP}{dx}\right), \qquad (s1)$$

where P denotes the pressure along the cylindrical vessel, dependent only on the axial coordinate x, and r represents the radial coordinate. The continuity equation and the angular equation of motion are identically satisfied. The viscosity of the blood, μ, was assumed to be a function of the hematocrit, based on the Saito model [3]

$$\mu = \mu_0\left[1 + \frac{2.5\phi}{(1-\phi)}\right], \qquad (s2)$$

where μ_0 denotes the viscosity of the solvent fluid and ϕ represents the red blood cell population density. Typically, for humans, ϕ is of the order of 40 – 45% [3]. The resulting velocity profile from equation (s1) is parabolic in nature. Using the definition for the flux, Q [4]

$$Q = \int_0^R 2\pi r\, u(r)dr, \qquad (s3)$$

the pressure gradient ΔP driving the flow is

$$\therefore \Delta P = \frac{8\mu LQ}{\pi R^4}. \quad (s4)$$

where R is the radius of the cylindrical blood vessel and L denotes its length.

Flux calculation: The conservation of flux for the parent-daughter bifurcation of Figure S1A without backflow can be written as

$$Q_{TOT} = Q_{L1} + Q_{R1}. \quad (s5)$$

Furthermore, the continuity of pressure at the bifurcation node can be expressed as

$$P^* = P_{L1} + \frac{8\mu L_{L1}Q_{L1}}{\pi R_{L1}^4} = P_{R1} + \frac{8\mu L_{R1}Q_{R1}}{\pi R_{R1}^4}, \qquad (s6)$$

where L_{L1}, L_{R1} and R_{L1}, R_{R1} are the respective lengths and radii of the daughter vessels. The daughter fluxes Q_{L1} and Q_{R1} are unknown but can be determined algebraically in terms of a known input flux, Q_{TOT}. To determine Q_{L1} and Q_{R1} we need to rewrite equation (s6) in terms of the respective daughter vessel's total impedance via Ohm's law. This results in

$$Z_{L1}Q_{L1} + \frac{8\mu L_{L1}Q_{L1}}{\pi R_{L1}^4} = Z_{R1}Q_{R1} + \frac{8\mu L_{R1}Q_{R1}}{\pi R_{R1}^4}, \qquad (s7)$$

where Z_{L1} and Z_{R1} represent the total impedance of the respective daughter blood vessels of Figure S1A and are given mathematically by equation (10) in the manuscript. Using equations (10), (s5) and (s7), we can algebraically determine the daughter fluxes Q_{L1} and Q_{R1} in terms of the parent flux Q_{TOT} for the given physical parameters shown in Table S1. The fluxes for the Hagen-Poiseuille model without backflow case were Q_{L1} = 300.275ml/min and Q_{R1} =299.725ml/min as shown in Table S3.

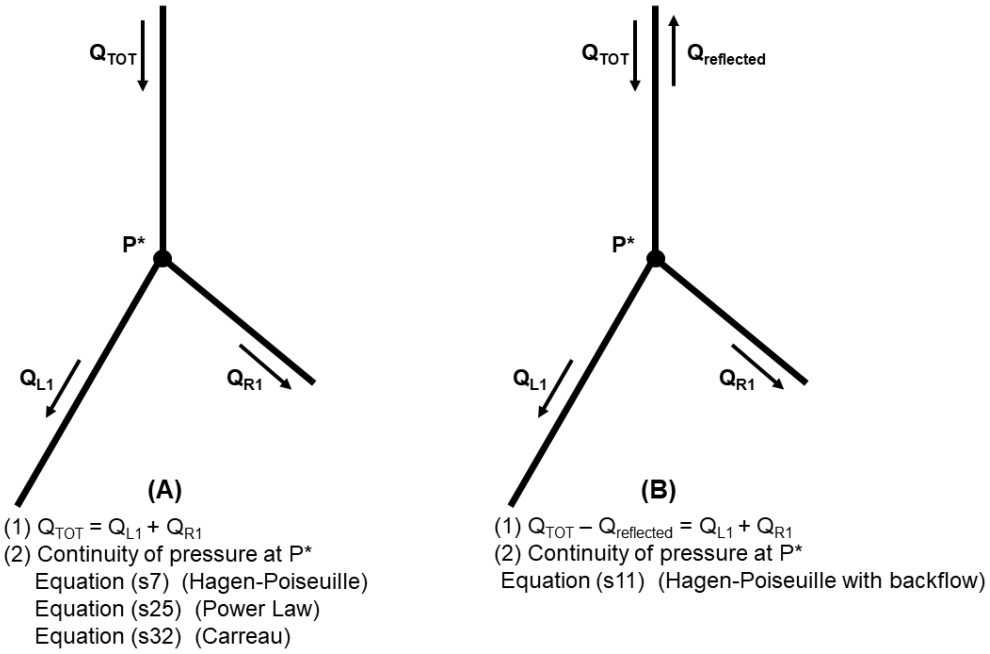

Figure S1. A single-node parent-daughter bifurcation (A) without backflow and (B) with backflow. P* denotes the pressure at the bifurcation node.

Table S1. Physical parameters for the various fluid models examined in the single-node bifurcation of Figure S1.

Physical parameter	Physical parameter notation	Value	Reference
Parent vessel radius	R	2.7×10^{-3}m	Cury et al. [5]
Left daughter vessel radius	R_{L1}	2.5×10^{-3}m	
Right daughter vessel radius	R_{R1}	2×10^{-3}m	
Parent vessel length	L	4×10^{-2}m	
Left daughter vessel length	L_{L1}	4×10^{-2}m	
Right daughter vessel length	L_{R1}	2×10^{-2}m	
Viscosity term in Saito formula, equation (s2)	μ_0	4×10^{-3} Pas	Stark and Shuster [3]
Hematocrit	ϕ	0.40	
Frequency	f	10 Hz	Abu-Naser et al. [1], Hsu et al. [2]
Left daughter vessel's total impedance	Z_{L1}	3.316×10^{9}kgm^{-4}s^{-1}	
Right daughter vessel's total impedance	Z_{R1}	3.316×10^{9}kgm^{-4}s^{-1}	
Parent vessel's total impedance	Z_T	1.649×10^{9}kgm^{-4}s^{-1}	
Blood flux rate to a healthy human kidney	Q_{TOT}	600mlmin^{-1} (10^{-5}m^{3}s^{-1})	Lok et al. [6]
Viscosity for the Power law model	m	16.24×10^{-3} Pas	Bessonov et al. [7]
Index for the Power law model	n	0.7163	
Shear rate	$\dot{\gamma}$	600s^{-1}	
Relaxation time	λ	3.313s	
Carreau model – viscosity at zero shear rate	μ_0	0.056Pas	
Carreau model- viscosity at infinite shear rate	μ_∞	0.00345Pas	
Index for the Carreau model	n	0.3568	

Table S2. Individual impedances and compliances for the three element Windkessel model for the single-node bifurcation cases of Figure S1.

Branch	**Z_1(kgm^{-4}s^{-1})**	**Z_2(kgm^{-4}s^{-1})**	**C(kg^{-1}m^{4}s^2)**	**|Z| (kgm^{-4}s^{-1})**
Parent vessel	1.180×10^9	4.830×10^8	1.840×10^{-12}	1.649×10^9
Left daughter branch L1	6.136×10^9	2.512×10^9	9.568×10^{-12}	3.316×10^9
Right daughter branch R1	6.136×10^9	2.512×10^9	9.568×10^{-12}	3.316×10^9

Table S3. Daughter fluxes for the sensitivity analysis for the various asymmetric single-node parent-daughter bifurcation models.

Fluid model	**Branch Q_{L1} (ml/min)**	**Branch Q_{R1} (ml/min)**
Hagen-Poiseuille without backflow	300.275	299.725
Hagen-Poiseuille with backflow	296.245	295.702
Power law without backflow	300.004	299.996
Carreau without backflow	299.749	300.251

S1.2 Hagen-Poiseuille model with backflow

Using Figure S1B, we apply the conservation of flux and the continuity of pressure at the bifurcation node which results in the following sets of equations,

$$Q_{TOT} - Q_{reflected} = Q_{L1} + Q_{R1}, \quad (s8)$$

and

$$P^* = P_{TOT} - \frac{8\mu L Q_{TOT}}{\pi R^4} + P_{reflected} + \frac{8\mu L Q_{TOT}}{\pi R^4}$$

$$= P_{L1} + \frac{8\mu L_{L1} Q_{L1}}{\pi R_{L1}^4} = P_{R1} + \frac{8\mu L_{R1} Q_{R1}}{\pi R_{R1}^4}, \qquad (s9)$$

where the pressures are related to the total impedance of each vessel via Ohm's law. Let

$$\alpha_{TOT} = \frac{8\mu L}{\pi R^4}, \qquad \alpha_{L1} = \frac{8\mu L_{L1}}{\pi R_{L1}^4}, \qquad \alpha_{R1} = \frac{8\mu L_{R1}}{\pi R_{R1}^4},$$

thus equation (s9) can be rewritten as

$$P^* = [Z_{TOT} - \alpha_{TOT}]Q_{TOT} + [Z_{TOT} + \alpha_{TOT}]Q_{reflected} = [Z_{L1} + \alpha_{L1}]Q_{L1} = [Z_{R1} + \alpha_{R1}]Q_{R1} \quad (s10).$$

Equation (s10) is rearranged resulting in

$$Q_{reflected} = Q_{TOT} \frac{[(Z_{R1} + \alpha_{R1})(Z_{L1} + \alpha_{L1}) - (Z_{TOT} - \alpha)(Z_{L1} + \alpha_{L1}) - (Z_{TOT} - \alpha)(Z_{R1} + \alpha_{R1})]}{[(Z_{R1} + \alpha_{R1})(Z_{L1} + \alpha_{L1}) + (Z_{TOT} + \alpha)(Z_{L1} + \alpha_{L1}) + (Z_{TOT} + \alpha)(Z_{R1} + \alpha_{R1})]} \quad (s11)$$

Using the appropriate physical data given in Table S1, we can determine the various fluxes for the Hagen-Poiseuille backflow model shown in Figure S1B. The fluxes for this case were Q_{L1} = 296.245ml/min and Q_{R1} = 295.702ml/min (see Table S3) which is approximately 1.4% lower in magnitude than the fluxes for the Hagen-Poiseuille without backflow.

S1.3 The power law fluid model

Using the Navier-Stokes equation in cylindrical coordinates, we can show that the Cauchy stress, σ, leads to [7,8]

$$\frac{1}{r}\frac{\partial}{\partial r}(r\sigma) = \frac{dP}{dx},$$

$$\sigma = \frac{r}{2}\left(\frac{dP}{dx}\right) + \frac{c_1}{r}, \qquad (s12)$$

where c_1 denotes a constant of integration. Since we require a physical model $c_1 \to 0$ as $r \to 0$. This results in

$$\sigma = \frac{r}{2}\left(\frac{dP}{dx}\right). \quad (s13)$$

The pressure gradient can be written as

$$\frac{dP}{dx} = \frac{\Delta P}{L}. \quad (s14)$$

Using equations (s13) and (s14), we get

$$\sigma = \frac{r\Delta P}{2L}. \quad (s15)$$

The viscosity of the fluid is given by $\sigma = m\left(\frac{du}{dr}\right)^n$, (s16)

where $du/dr = \dot{\gamma}$, and $\dot{\gamma}$ is defined as the shear strain rate [7,8]. Combining equations (s15) and (s16), we can show that

$$\frac{du}{dr} = \left(\frac{\Delta P}{2mL}\right)^{\frac{1}{n}} r^{\frac{1}{n}}. \quad (s17)$$

Integrating equation (s17) between the radial position r, to the vessel radius R, we can describe the velocity profile u as

$$u = \frac{1}{(1+1/n)}\left(\frac{\Delta P}{2mL}\right)^{\frac{1}{n}}\left(R^{1/(1+n)} - r^{1/(1+n)}\right). \quad (s18)$$

Calculating the flux, Q, where the flux is defined as (s3)

results in

$$Q = \frac{\pi}{(3+1/n)}\left(\frac{R}{2mL}\right) R^3 \Delta P^{\frac{1}{n}}. \quad (s19)$$

Defining the material parameter α as

$$\alpha = \frac{\pi}{(3+1/n)}\left(\frac{R}{2mL}\right)^{\frac{1}{n}} R^3, \quad (s20)$$

allows us to write the pressure difference ΔP as

$$\Delta P = \beta Q^n, \quad (s21)$$

where $\beta = 1/\alpha^n$. We can relate the pressure difference ΔP to the pressure at the bifurcation node denoted by P^*, and the pressure within the individual blood vessel which is represented by P, via $\Delta P = P^* - P$. Using Ohm's law gives

$$P^\star = \beta Q^n + ZQ. \quad (s22)$$

Considering the simple parent-daughter bifurcation described in Figure S1A and using equation (s22) along with the conservation of flux leads to the following system of equations

$$Q_{TOT} = Q_{L1} + Q_{R1}, \quad (s23)$$

$$P^\star = Z_{L1}Q_{L1} + \beta_{L1}Q_{L1}^n = Z_{R1}Q_{R1} + \beta_{R1}Q_{R1}^n. \quad (s24)$$

Using equation (s24) and substituting in the conservation of flux for Q_{R1} from equation (s23) results in

$$\beta_{L1}Q_{L1}^n - \beta_{R1}(Q_{TOT} - Q_{L1})^n + (Z_{L1} + Z_{R1})Q_{L1} - Z_{R1}Q_{TOT} = 0. \quad (s25)$$

Equation (s25) reduces to a root finding problem which we can solve numerically using Mathematica© [9] and the appropriate material parameters given in Table S1. The fluxes for the fluid Power law were Q_{L1} = 300.004ml/min and Q_{R1} = 299.996ml/min (see Table S3) which is very close in magnitude to the fluxes associated with the Hagen-Poiseuille model without backflow.

S1.4 The Carreau fluid model for an asymmetric parent-daughter bifurcation

A key physical feature of blood is its shear thinning characteristics which we can model using the non-linear Carreau model [7,8]. The Carreau model has less physical limitations than the power law model,

with the power law model predicting an unbounded viscosity at zero shear rate and zero viscosity when $\dot{\gamma} \to \infty$, which is essentially unphysical in nature. The Carreau model is given by the equation

$$\mu = \mu_\infty + (\mu_0 - \mu_\infty)\left(1 + \lambda^2\dot{\gamma}^2\right)^{\frac{n-1}{2}}, \quad (s26)$$

where μ_0 and μ_∞ represent the viscosities at the respective physical boundaries and n is a non-dimensional number obtained empirically. The terms λ and $\dot{\gamma}$ represent the relaxation term and the shear strain rate respectively. The shear strain rate for a typical unblocked artery is $\dot{\gamma}$= 600s^{-1}, the relaxation time is λ = 3.313s, μ_0 = 0.056Pas, μ_∞ = 0.00345Pas and n = 0.3568 [7]. The viscosity μ is related to the Cauchy stress σ via

$$\sigma = \mu\dot{\gamma}. \quad (s27)$$

Using equations (s15), (s26) and (s27), and rearranging we get

$$\Delta P = \left(\frac{2L}{r}\right)\dot{\gamma}\left[\mu_\infty + (\mu_0 - \mu_\infty)\left(1 + \lambda^2\dot{\gamma}^2\right)^{\frac{n-1}{2}}\right], \quad (s28)$$

where $\Delta P = P^* - P$. Using Ohm's law and rearranging equation (s28) leads to

$$P^\star = ZQ + \left(\frac{2L}{r}\right)\dot{\gamma}\left[\mu_\infty + (\mu_0 - \mu_\infty)\left(1 + \lambda^2\dot{\gamma}^2\right)^{\frac{n-1}{2}}\right]. \quad (s29)$$

Applying the conservation of flux and the continuity of pressure at the bifurcation point for Figure S1A, results in the following system of equations

$$Q_{TOT} = Q_{L1} + Q_{R1}, \quad (s30)$$

$$\begin{aligned} P^\star &= Z_{L1}Q_{L1} + \left(\frac{2L_{L1}}{R_{L1}}\right)\dot{\gamma}\left[\mu_\infty + (\mu_0 - \mu_\infty)\left(1 + \lambda^2\dot{\gamma}^2\right)^{\frac{n-1}{2}}\right] \\ &= Z_{R1}Q_{R1} + \left(\frac{2L_{R1}}{R_{R1}}\right)\dot{\gamma}\left[\mu_\infty + (\mu_0 - \mu_\infty)\left(1 + \lambda^2\dot{\gamma}^2\right)^{\frac{n-1}{2}}\right], \quad (s31) \end{aligned}$$

Using equations (s30) and (s31) and rearranging, yields

$$Z_{L1}Q_{L1} - Z_{R1}(Q_{TOT} - Q_{L1}) + 2\dot{\gamma}\left(\frac{L_{L1}}{R_{L1}} - \frac{L_{R1}}{R_{R1}}\right)\left[\mu_\infty + (\mu_0 - \mu_\infty)\left(1 + \lambda^2\dot{\gamma}^2\right)^{\frac{n-1}{2}}\right] = 0. \quad (s32)$$

We solved equation (s32) using Mathematica© [9] alongside the physical data given in Table S1. The fluxes for the Carreau model were Q_{L1} = 299.749ml/min and Q_{R1} = 300.251ml/min (see Table S3) which was very close in magnitude to the fluxes associated with the Hagen-Poiseuille model without backflow and the power law fluid model. However, the left branch L1 in the Carreau model had a slightly lower blood flux compared to the right branch, whereas both the Hagen-Poiseuille model without backflow and the power law fluid model exhibited slightly larger blood fluxes in the right branch compared to the left branch.

The data from this sensitivity analysis illustrate that the effects of backflow ($Q_{reflection}$) were so small as to be negligible, being approximately 1.4% of the total flux Q_{TOT}. There was little difference between the flow rates for the Hagen-Poiseuille fluid model with a constant viscosity, the power law, and the Carreau model. It is worth noting that the Carreau model is dependent on the shear strain rate which influences the viscosity of blood, with higher shear strain rates resulting in a lower blood viscosity. We therefore primarily focused on the Carreau model without backflow when calculating the blood fluxes and blood losses that arise from the kidney vasculature of Figure 1A. Focusing on the Carreau

model rather than the Newtonian model offers more flexibility since it allows to account for shear thinning effects and varying shear rates.

S2 Sensitivity analysis for the parameter space of a simple Y bifurcation

Tables discussed in the main text in Section 2.4

Table S4. Sensitivity analysis for the radius r_{L1} using the data from Tables S1 & S2.

r_{L1} (m)	Q_{L1} (ml/min)	Q_{R1} (ml/min)
2.5 x10^{-3}	299.749	300.251
2.0 x10^{-3}	299.582	300.418
1.5 x10^{-3}	299.304	300.696
1.0 x10^{-3}	298.747	301.253

Table S5. Sensitivity analysis for the length L_{L1} using the data from Tables S1 & S2.

L_{L1} (m)	Q_{L1} (ml/min)	Q_{R1} (ml/min)
4 x10^{-2}	299.749	300.251
3 x10^{-2}	299.917	300.083
2 x10^{-2}	300.083	299.917
1 x10^{-2}	300.251	299.749
5 x10^{-3}	300.334	299.666

Table S6. Sensitivity analysis for the shear rate, $\dot{\gamma}$, using the data from Tables S1 & S2.

$\dot{\gamma}$ (s^{-1})	Q_{L1} (ml/min)	Q_{R1} (ml/min)
100	299.949	300.051
600	299.749	300.25
1000	299.594	300.406
2000	299.211	300.789
5000	298.072	301.928
10000	296.184	303.816

Table S7. Sensitivity analysis for the hematocrit ϕ, using the data from Tables S1 & S2.

ϕ	Q_{L1} (ml/min)	Q_{R1} (ml/min)
0.35	300.242	299.758
0.40	300.275	299.725
0.45	300.314	299.686
0.50	300.36	299.64
0.55	300.416	299.584

Table S8 Sensitivity analysis for the impedance Z_{L1} using the data from Tables S1 & S2

Z_{L1} ($kgm^{-4}s^{-1}$)	Q_{L1} (ml/min)	Q_{R1} (ml/min)
3.3×10^9	300.473	299.527
3.4×10^9	295.999	304.001
3.5×10^9	291.656	308.344
3.6×10^9	287.440	312.560
3.7×10^9	283.342	316.658
3.8×10^9	279.361	320.639
3.9×10^9	275.489	324.511
4.0×10^9	271.724	328.276

References

1. Abu-Naser M, Williamson GA, Bidani AK, Griffin KA. Vascular resistance estimation in real hemodynamics using a time-varying Windkessel model. IEEE- ICASSPl. 2005;5:641-4.
2. Hsu TL, Hsiu H, Chao PT, Li SP, Wang WK, Wang YYL. Three-block electrical model of renal impedance. IOP: Physiological measurement. 2005;26(4):387-99.
3. Stark H, Schuster S. Comparison of various approaches to calculating the hematocrit in vertebrates. Journal of applied physiology. 2012;113(3):355-67.
4. Grinberg L, Karniadakis GE. Outflow boundary conditions for arterial networks with multiple outlets. Annals of biomechanical engineering. 2008;36(9):1496-514.
5. Cury LFM, Talou GM, Younes-Ibrahim M, Blanco PJ. Parallel generation of extensive vascular networks with application to an archetypal human kidney model. Royal Society Open Science. 2021;8(12):1-22.
6. Lok CE, Huber TS, Lee T, Shenoy S, Yevzlin AS, Abreo K, et al. Kdoqi clinical practice guideline for vascular access: 2019 update. American journal of kidney diseases. 2020;75(4):1-164.
7. Bessonov N, Sequeira A, Simakov S, Vassilevskii Y, Volpert V. Methods of blood flow modelling. Mathematical Modelling of Natural Phenomena. 2016;11(1):1-25.
8. Sochi T. Analytical solutions for the flow of Carreau and Cross fluids in circular pipes and thin slits. Rheologica Acta. 2015;54:745-56.
9. Wolfram Research Inc. Mathematica. Version 130. 2022.